REPORT DOCUMENTATION PAGE

Form Approved
OMB No. 0704-0188

1. REPORT DATE *(DD-MM-YYYY)*	2. REPORT TYPE	3. DATES COVERED *(From - To)*
07-08-2008	Journal Article	

4. TITLE AND SUBTITLE
Modeling the Circulation of the Atchafalaya Bay System Part 2: River Plume Dynamics During Cold Fronts

5a. CONTRACT NUMBER

5b. GRANT NUMBER

5c. PROGRAM ELEMENT NUMBER
0601153N

6. AUTHOR(S)
Carolus M. Cobb, Timothy Keen, Nan Walker

5d. PROJECT NUMBER

5e. TASK NUMBER

5f. WORK UNIT NUMBER
73-8544-B7-5

7. PERFORMING ORGANIZATION NAME(S) AND ADDRESS(ES)
Naval Research Laboratory
Oceanography Division
Stennis Space Center, MS 39529-5004

8. PERFORMING ORGANIZATION REPORT NUMBER
NRL/JA/7320-07-7131

9. SPONSORING/MONITORING AGENCY NAME(S) AND ADDRESS(ES)
Office of Naval Research
800 N. Quincy St.
Arlington, VA 22217-5660

10. SPONSOR/MONITOR'S ACRONYM(S)
ONR

11. SPONSOR/MONITOR'S REPORT NUMBER(S)

12. DISTRIBUTION/AVAILABILITY STATEMENT
Approved for public release, distribution is unlimited.

13. SUPPLEMENTARY NOTES

14. ABSTRACT

In Part 2 of our application of the Navy coastal ocean model (NCOM) to the Atchafalaya Bay system, we examine the wind- and tide-forced three-dimensional baroclinic circulation of the Lower Atchafalaya and Wax Lake Outlet river plumes. The salinity and the current velocity are examined during a time period when three cold fronts passed over the region. The baroclinic circulation of NCOM was validated for the same time period in Part 1 of this study (Cobb, Keen, and Walker, 2008. Modeling the circulation of the Atchafalaya Bay region, 1: Model description and validation. Journal of Coastal Research, this issue). We find that the . . .

15. SUBJECT TERMS

coastal processes, Atchafalaya Bay system, river plume, salinity front, sedimetn transport, remote sensing, NCOM, cold front

16. SECURITY CLASSIFICATION OF:			17. LIMITATION OF ABSTRACT	18. NUMBER OF PAGES	19a. NAME OF RESPONSIBLE PERSON
a. REPORT	b. ABSTRACT	c. THIS PAGE			Timothy Keen
Unclassified	Unclassified	Unclassified	UL	14	19b. TELEPHONE NUMBER *(Include area code)* 228-688-4950

Journal of Coastal Research	24	4	1048–1062	West Palm Beach, Florida	July 2008

Modeling the Circulation of the Atchafalaya Bay System. Part 2: River Plume Dynamics during Cold Fronts

Mark Cobb[†], Timothy R. Keen[‡], and Nan D. Walker[§]

[†]Naval Oceanographic Office, Code NP1
Stennis Space Center, MS 39529, U.S.A.
carolus.cobb@navy.mil

[‡]Oceanography Division
Naval Research Laboratory, Code 7320
Stennis Space Center, MS 39529, U.S.A.

[§]Louisiana State University
Department of Oceanography and Coastal Sciences
Coastal Studies Institute
Louisiana State University, Baton Rouge, LA 70803, U.S.A.

ABSTRACT

COBB, M.; KEEN, T.R., and WALKER, N.D., 2008. Modeling the circulation of the Atchafalaya Bay system, part 2: River plume dynamics during cold fronts. *Journal of Coastal Research*, 24(4), 1048–1062. West Palm Beach (Florida), ISSN 0749-0208.

In Part 2 of our application of the Navy coastal ocean model (NCOM) to the Atchafalaya Bay system, we examine the wind- and tide-forced three-dimensional baroclinic circulation of the Lower Atchafalaya and Wax Lake Outlet river plumes. The salinity and the current velocity are examined during a time period when three cold fronts passed over the region. The baroclinic circulation of NCOM was validated for the same time period in Part 1 of this study (COBB, KEEN, and WALKER, 2008. Modeling the circulation of the Atchafalaya Bay region, 1: Model description and validation. *Journal of Coastal Research*, this issue). We find that the westward transport of plume water and the offshore cold-front–induced circulation are determined to a large extent by the alongshore and cross-shore bathymetric structure. Wind-driven plume water moves parallel to the alongshore bathymetric contours unless forced to mix with higher salinity water by strong cross-shore directed winds. The mixing of plume water with offshore water occurs over bathymetric shoals during periods of strong post-frontal winds. This mixing process involves the offshore transport of plume water over the entire water column in addition to the strong surface transport. The model results for offshore circulation are in qualitative agreement with past observations. In addition, the hydrodynamic processes that control the salinity fronts in Vermilion and West Cote Blanche Bays, areas where the model salinity was validated in Part 1, are examined as well.

ADDITIONAL INDEX WORDS: *Coastal processes, Atchafalaya Bay system, river plume, salinity front, sediment transport, remote sensing, NCOM, cold front.*

INTRODUCTION

The 1500 km² Atchafalaya Bay system (Figure 1) is one of the most dynamic regions of the Louisiana coast, with large influxes of freshwater (15% to 29% of the total Mississippi River; ALLISON *et al.*, 2000; WALKER and HAMMACK, 2000) from the Lower Atchafalaya River (LAR) and Wax Lake Outlet (WLO). These rivers transport 40% to 50% of the total Mississippi sediment load (MOSSA and ROBERTS, 1990) and thus have a great impact on the bathymetry and coastline of the region. A new phase of delta building began in the 1950s, creating subaerial deltas at the mouths of the LAR and WLO (ROBERTS, ADAMS, and CUNNINGHAM, 1980; SCHLEMON, 1975). Many studies over the last 30 years have focused on the sediment transport of these river plumes and their impact on the Chenier Plain, which is west of the Atchafalaya Bay system (DRAUT *et al.*, 2005b; HUH *et al.*, 1991; ROBERTS *et al.*, 1989; VAN HEERDEN and ROBERTS, 1980; WALKER and HAMMACK, 2000; WELLS and KEMP, 1981). The coastline of the Chenier Plain is actually prograding at a rate of 29 to 50 m y^{-1} due to the large volume of fine grain sediment transported to the west by the Atchafalaya mud stream (DRAUT *et al.*, 2005a; HUH, WALKER, and MOELLER, 2001).

DOI: 10.2112/07-0879.1 received 24 April 2007; accepted in revision 16 November 2007.

Background

It has been discovered that atmospheric cold fronts play a significant role in determining the overall sediment transport within the region through their influence on the motion of the LAR and WLO river plumes (hereafter referred to as the river plume) as well as on the coastal wave environment (ALLISON *et al.*, 2000; DRAUT *et al.*, 2005a; HUH, WALKER, and MOELLER, 2001; KEMP, WELLS, and VAN HEERDEN, 1980; KINEKE *et al.*, 2006; MOELLER *et al.*, 1993; PEREZ *et al.*, 2000; WALKER and HAMMACK, 2000). Twenty to 30 cold fronts pass through this region between October and April, with 4 to 7 days between each frontal passage (KAHN and ROBERTS, 1982). The strong, variable winds associated with a cold front influence the circulation throughout the region and generate surface waves that resuspend sediment in the vicinity of Atchafalaya Bay (ALLISON *et al.*, 2000; WALKER and HAMMACK, 2000). The post-frontal northerly winds cause set down of coastal water levels (increasing the effectiveness of waves in

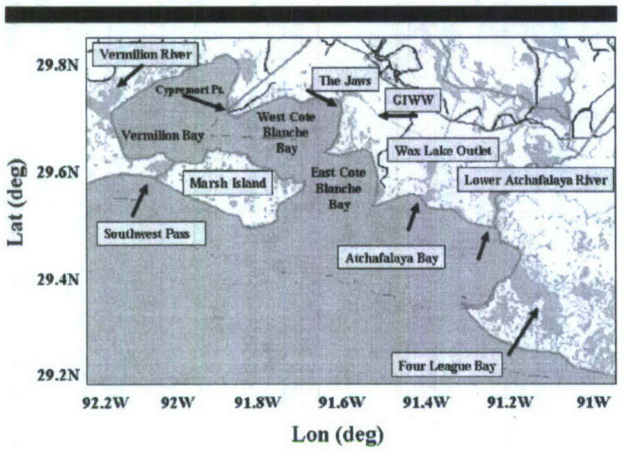

Figure 1. Regional map showing Atchafalaya Bay system and locations referred to in the text. GIWW = gulf intracoastal waterway.

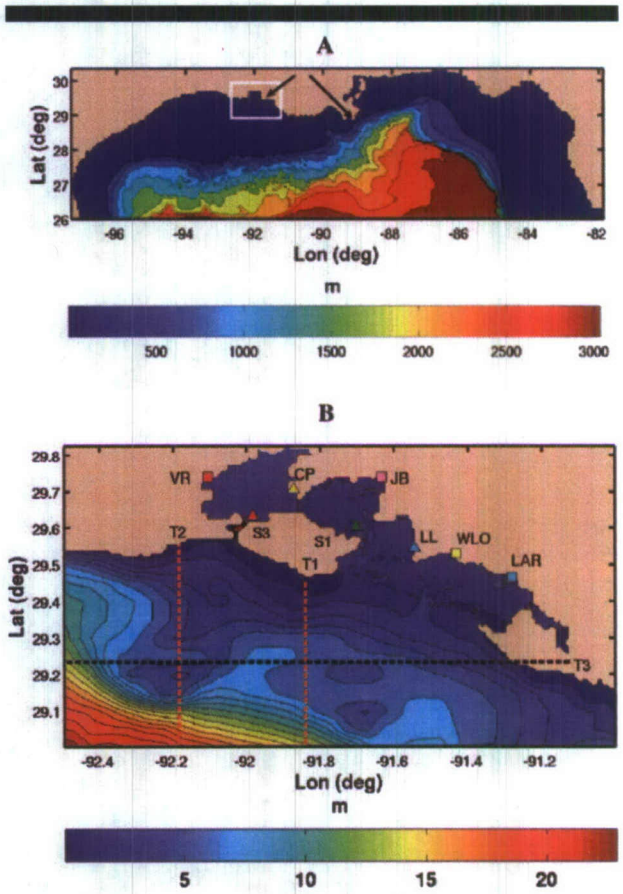

Figure 2. (A) Northern Gulf of Mexico (NGOM) grid bathymetry. The contour spacing is approximately 300 m. The region enclosed by the white square is the location of the nested Atchafalaya Bay grid, and the arrows indicate the locations of the Atchafalaya and Mississippi River inflows. (B) Bathymetry, inflow points, and data locations of the Atchafalaya Bay system. Contour spacing is 1 m. The squares indicate sources of freshwater: LAR = lower Atchafalaya River; WLO = Wax Lake outlet; JB = Jaws Bay; VR = Vermilion River (VR). Data (salinity, current velocity) location points from Walker and Hammack (2000) are indicated by triangles: S1 = site 1; S3 = site 3; CP = Cypremort Point; LL = Luke's Landing. The two vertical dashed red lines (T1 and T2) indicate the locations of the cross-shore transects. The horizontal dashed black line (T3) indicates the location of the alongshore transect.

sediment resuspension) and force the river plume to the south–southeast, reversing the normally westward transport of sediment along the coast (HUH, WALKER, and MOELLER, 2001; WALKER and HAMMACK, 2000; WELLS and KEMP, 1981). The river plume circulation and sediment transport have been observed through remotely sensed imagery and investigated through field studies (ALLISON *et al.*, 2000; HUH, WALKER, and MOELLER, 2001; KINEKE *et al.*, 2006; MOELLER *et al.*, 1993; WALKER and HAMMACK, 2000; WALKER, 2001; WALKER *et al.*, 2002), but there remain several aspects of the large-scale wind-driven circulation that need to be quantified through both observation and modeling studies.

In order to have a more comprehensive understanding of the circulation and sediment transport processes along the Louisiana coast during cold fronts and hurricanes, it is essential that numerical models be applied. The circulation and sedimentation of the Atchafalaya Bay system has been studied for many years using both measurements and remote sensing studies, but not with numerical models. Therefore, an important first step toward predicting sediment transport in this region is to accurately model its hydrodynamics. Our previous study (COBB, KEEN, and WALKER, 2008; hereafter CKW1) focused on validating the baroclinic hydrodynamics of the Navy coastal ocean model (NCOM) (BARRON *et al.*, 2004; KARA *et al.*, 2006) within the Atchafalaya Bay complex but did not investigate the circulation processes on the shelf and within the bays.

Objectives

The primary objective of this study is to examine the wind-, tide-, and river-forced circulation patterns of the Atchafalaya Bay system during the passage of multiple cold fronts using a numerical modeling approach. The Navy coastal ocean model has been validated for the December 23, 1997, and January 11, 1998, interval, during which three cold fronts passed over the region (CKW1). This study complements our previous work by focusing on the large-scale motion of the river plume during a cold-front event as well as the westward transport of plume water that occurs between cold fronts. In addition, the vertical structure of the salinity and the currents will be investigated in order to characterize the three-dimensional dynamics of the circulation.

The response of the salinity in Vermilion and West Cote Blanche Bays (see CKW1) to wind forcing will be examined as well at the same locations (sites 1 and 3 from WALKER and HAMMACK 2000, hereafter WH00) that the model was validated at in CKW1 (see Figure 2B). In addition, time series of the water level, current velocity, and salinity will be examined at these sites. The purpose of the time series analysis is to determine what circulation processes control the salinity changes at sites 1 and 3 and how they are influenced by the passage of a cold front.

METHODS

The Navy Coastal Ocean Model (NCOM)

The Navy coastal ocean model is a three-dimensional, primitive equation, hydrodynamic model that employs the hydrostatic, incompressible, and Boussinesq approximations to solve the conservation equations for the flow velocity, temperature, and salinity. It also includes the standard continuity equation for mass (MOREY *et al.*, 2003). It uses Smagorinsky horizontal mixing coefficients and the Mellor-Yamada level 2.5 parameterization for vertical mixing. The model equations are solved on an Arakawa C grid. The horizontal grid is curvilinear and uses a hybrid vertical coordinate system, which consists of both fixed z levels in deep water and variable σ coordinates in shallow water. The free surface and vertical mixing equations are solved implicitly; the other terms are treated explicitly. The Navy coastal ocean model can be nested to a coarse-grid model to supply boundary conditions at the open boundary of the domain. The Navy coastal ocean model has been validated at global (BARRON *et al.*, 2004; KARA *et al.*, 2006) and basin scales (KO, PRELLER, and MARTIN, 2003). It also compares well with observations from coastal regions (*e.g.*, CKW1; KEEN *et al.*, 2006; MOREY *et al.*, 2003).

The surface boundary condition for all of the simulations discussed herein consists of wind speed and direction at 6-hour intervals interpolated from the 1° Navy Global Operational Atmospheric Prediction System (NOGAPS) forecast fields. Open boundary conditions for NCOM comprise water levels and vertically integrated transports, which can consist of separate subtidal and tidal flows, as well as profiles of temperature, salinity, and currents. A radiation boundary condition is used for momentum, heat, and mass along the open boundary. River inflow is represented by a boundary condition for transport, temperature, and salinity at specified grid cells. Specific boundary conditions for the simulations discussed in this paper are described below.

The Navy coastal ocean model is run on two domains for this study (Figure 2): (1) A Northern Gulf of Mexico (NGOM) grid with a model cell resolution of approximately 5 km and (2) a smaller nested Atchafalaya Bay domain grid (ABG) with a model cell resolution of ~800 m. In the first part of this study (CKW1), the specific details of the nesting, initial conditions, boundary conditions, bathymetry, tide, wind, and river forcing were discussed, and the reader is referred to this paper for more information regarding the model setup. In this section we give a very brief description of the ABG model simulation.

The Atchafalaya Bay Simulations

The ABG grid has 188 and 125 computational nodes in the x and y directions, respectively. All of the ABG simulations in this study use four z levels and four terrain-following σ levels with a minimum depth of 1 m. The σ levels are applied when the depth is less than 15 m. The ABG open boundary conditions during the study interval are interpolated from the NGOM 3-hour output fields of water level, temperature, salinity, and currents (see CKW1). The wind velocity fields used for the ABG simulations are interpolated from the NOGAPS output at 6-hour intervals. Time series for the wind vectors and their magnitudes at Cypremort Point are shown in Figure 3.

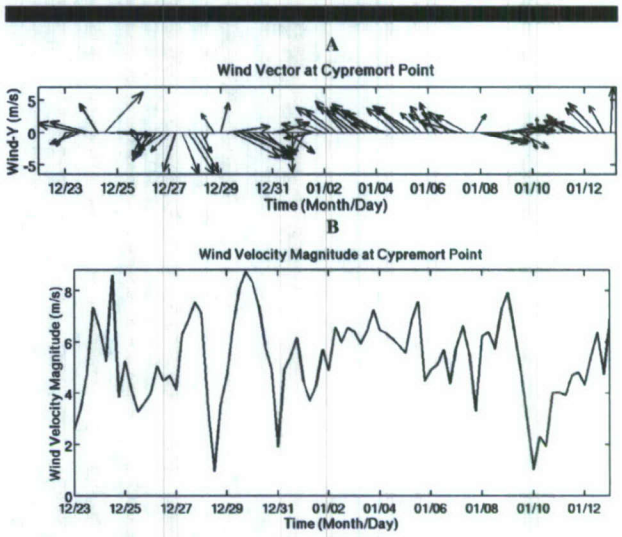

Figure 3. Interpolated NOGAPS forecast at Cypremort Point (91.87°W, 29.71°N) between December 23, 1997, and January 12, 1998. (A) Wind vectors. (B) Wind vector magnitudes.

The ABG simulation includes five sources of freshwater. The primary sources for the river plume water are the LAR and WLO (see Figure 2B for the locations of their outflow points). In addition, the Jaws Bay and Cypremort Point gulf intracoastal waterway (GIWW) outlets (see Figure 2B) are also included since they play an important role in determining the salinity levels of the western bays. The Vermilion River (see Figure 2B) is included as well because of its influence on a location at which salinity was measured by WH00. The temperature, salinity, and discharge rates were determined from several sources and adjusted accordingly to match the data of WH00 as part of the model validation (see CKW1). Since data on freshwater inflow to Four League Bay were not available for this study, the results presented herein contain a patch of high-salinity water that is an artifact of the initial conditions used to spin up the model (see CKW1 for details).

RIVER PLUME DYNAMICS

This section presents the current and salinity patterns of the river plume for the December 23 to 30, 1997, time period. Two cold fronts passed over the region during this time, the first one on December 25 and the second on December 29.

Westward Transport of the River Plume

Southeasterly to northeasterly winds are dominant along the Louisiana coast during most of the year, except for the summer months when relatively weak southwesterly winds occur (WH00). The easterly winds force the river plume to the west and produce the Atchafalaya mud stream (ROBERTS

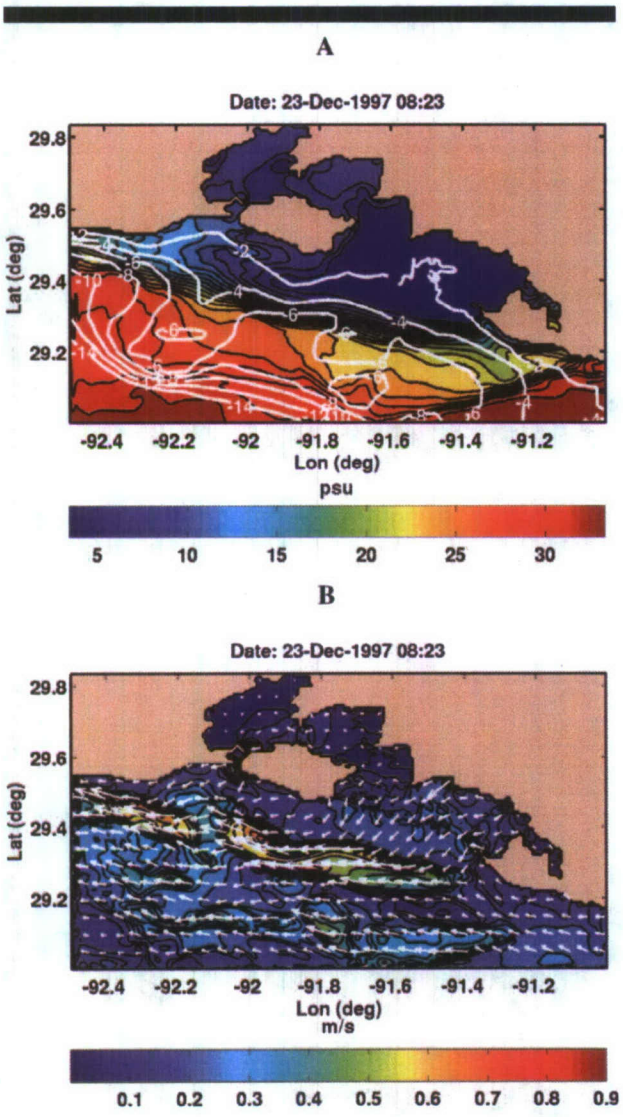

Figure 4. (A) Surface salinity contours on December 23 (0823 hours), 1997, just prior to the first cold front. Bathymetry (m) contours are plotted in white from −2- to −14-m depth with a 2-m interval. (B) Surface current velocity direction and magnitude. Every 6th current vector is plotted.

et al., 1987; WELLS and KEMP, 1981). This section presents results for the three-dimensional salinity and current velocity structure during the westward transport of the river plume.

Surface Circulation and Salinity

The wind velocity prior to the cold front on December 23 was northeasterly at 4–6 m s^{-1}, and the resultant river plume from the model (Figure 4A) shows the typical prefrontal westward circulation of the region. An isobath-parallel salinity front near the coast separates offshore water from 4-psu plume water (Figure 4B); note that the surface currents are shown in Figure 4B. The freshwater plume remains within the 6-m isobath and does not initially mix with the offshore water. The salinity ranges from 8 to 33 psu within an intermediate mixing zone between 4- and 14-m depths in the vicinity of Atchafalaya Bay. The plume salinity increases to 15 psu by entraining shelf water as it is transported to the west. The simulated plume narrows and remains within the 10-m isobath as it moves westward.

The river plume currents, which are initially directed to the southwest at the entrance to Atchafalaya Bay, turn westward near the 4-m isobath. Currents of 0.6 m s^{-1} are predicted in a band between the 3- and 6-m water depths along the salinity front. The surface flow decreases between −92° and −92.2° (Figure 4B), where the distance between the 2- and 6-m depth contours increases (Figure 4A). The flow reintensifies to the west as this nearshore zone narrows, thus clearly demonstrating that the plume is constrained by baroclinic forces in conjunction with the alongshore and cross-shore bathymetry. Tidal currents do not disrupt the westward-directed plume currents because the tidal forcing is relatively weak.

The westward transport of the river plume predicted by NCOM has the same general characteristics predicted by other modeling studies (CHAPMAN and LENTZ, 1994; KOURAFALOU *et al.*, 1996; NARAYANAN and GARVINE, 2002; OEY and MELLOR, 1993; XING and DAVIES, 1999). The primary features to note are (1) the sharp salinity front, (2) the strong currents along the salinity front, and (3) the plume's response to the bathymetry. In particular, the simulated river plume has the general features of a surface-to-bottom type plume. Furthermore, the Coriolis force reinforces the westward deflection of the plume as it emerges from Atchafalaya Bay.

The salinity patterns (Figures 4A) are similar to remotely sensed images of surface sediment transported to the west from the Atchafalaya Bay region (HUH, WALKER, and MOELLER, 2001; MOELLER *et al.*, 1993; WH00; WALKER *et al.*, 2002). In particular, the narrowing of the river plume as it approaches the western boundary of the domain is consistent with the estimated sediment transport patterns from advanced very high resolution radiometry (AVHRR); see WH00 and CKW1 for a discussion of the relationship between salinity and suspended sediment concentration (SSC). Suspended sediment concentration values of 10–100 mg L^{-1} have been measured in depths of 5 to 10 m within the Atchafalaya mud stream in the Chenier Plain region (KINEKE *et al.*, 2006), near the western edge of the model domain. The observed cross-shore extent of the sediment plume is similar to that of the freshwater plume in the NCOM simulations.

Field measurements of the offshore salinity during a time period of southeasterly winds (KINEKE *et al.*, 2006) are in qualitative agreement with the model results of Figure 4A. These field measurements show that the plume front near Atchafalaya Bay is at the 5-m isobath and that the plume narrows to the west along the 10-m isobath. In addition, the observations also show that SSC rapidly decreases in the cross-shore direction as salinity increases. Because the river plume transports large quantities of sediment to the west, the low-salinity water of the plume is correlated with higher SSC.

Cross Sections of Currents and Salinity

Cross sections of salinity, easting velocity, and northing velocity (Figure 5) along cross-shore transects T1 and T2 (see Figure 2B for locations) demonstrate the vertical structure of the river plume during typical prefrontal conditions (December 23, 1997). A maximum depth of 6 m is used in the cross sections in order to focus on the river plume salinity front, which is constrained to shallower depths. The plume front extends throughout the water column west of the Atchafalaya Bay entrance (Figure 5A), but with some low-salinity water displaced further offshore at the surface and some shelf water intruding near the bottom. This structure is weaker at transect T2 (Figure 5B), which is located 35 km to the west. The shelf water intrudes at a height of approximately 1 m above the bottom at both transects. The plume front is located in a water depth of 5 m at T1 and 4 m at T2, suggesting that this is the equilibrium depth for the onshore buoyancy flux and vertical mixing. The front cannot move any farther offshore (CHAPMAN and LENTZ, 1994; NARAYANAN and GARVINE, 2002), and the plume moves parallel to the isobaths because of this trapping effect.

The salinity along transect T1 is in qualitative agreement with sections measured by ALLISON *et al.* (2000) in the vicinity of Marsh Island, which clearly show the stratification of the river plume front and its close proximity to the coast. In particular, their observations reveal that the plume does not extend offshore beyond 10 m and is mainly seen in depths of less than 6 m. The plume salinity predicted by the model at T1 and T2 (Figures 5A and 5B) is consistent with these observations and those of KINEKE *et al.* (2006) near the Chenier Plain region.

The surface coastal jet predicted by NCOM (Figure 4B) is restricted to the upper 1 m of the water column at transect T1 (Figure 5C), and the flow maintains this structure at transect T2 (Figure 5D). A comparison of the salinity and velocity transects shows that the jet is located along the plume front and that its shape corresponds to the plume front structure. The alongshore jet velocities are between 0.3 and 0.6 m s^{-1} and decrease to 0.25 m s^{-1} away from the salinity front. WALKER *et al.* (2002) reported sustained westward currents between ~0.3 and 0.5 m s^{-1} in response to southeasterly wind forcing of 7 m s^{-1} south of Marsh Island in 5 m of water; the average middepth velocity was determined to be 0.26 m s^{-1}. This surface jet at the plume front is exactly what one would expect from idealized plume dynamics, although the current structures for the Louisiana shelf are more complex than the idealized cases used in previous studies (CHAPMAN and LENTZ, 1994; NARAYANAN and GARVINE, 2002; XING and DAVIES, 1999).

Vertical changes in the velocity field are correlated with the salinity and, therefore, the structure of the front. For example, westward surface currents of 0.6 m s^{-1} at transect T1 weaken to less than 0.3 m s^{-1} below 1 m, where 25-psu shelf water is found, and increase to 0.5 m s^{-1} at depths of 2–4 m, where water with a salinity around 10 psu is moving offshore. The alongshore velocity vanishes or becomes slightly eastward within 1 m of the bottom, where higher salinity water is intruding (CHAPMAN and LENTZ, 1994). A similar pattern is also seen over the entire water column at transect T2. The structure of the alongshore velocity at T1 and T2 is also correlated with the cross-shore velocity. The simulated cross-shelf flow on the shoreward side of the front at transect T1 (Figure 5E) is directed seaward, and the flow on the seaward side of the front is landward. The pattern of cross-shelf flow at transect T2 (Figure 5F) is similar to that at T1, but the onshore flow at the surface exceeds 0.15 m s^{-1} and the offshore flow at T2 is more uniform on the shoreward side of the front. This vertical structure is consistent with observations of prefrontal alongshore and cross-shore currents (KINEKE *et al.*, 2006) as well as idealized plume studies (CHAPMAN and LENTZ, 1994).

Plume Dynamics during a Cold Front

The cold fronts on December 26 and 29, 1997, and January 8, 1998, are accompanied by clockwise rotation of the wind from southerly to northerly and strengthening of the post-frontal winds (Figure 3), followed by a weakening of the northerly wind. These rapid changes in wind speed and direction have important consequences for the evolution of the river plume and front.

Surface Flow and Salinity Patterns

The southwesterly prefrontal NOGAPS winds rotate to westerly on December 25, 1997 (Figure 3A), thereby pushing the predicted river plume to the southeast corner of the domain (Figure 6A) and allowing some shelf water to replace low-salinity water in the western part of the domain. The plume begins moving offshore and mixes with higher salinity water in the southeast. The strongest surface currents (Figure 7A) are associated with the salinity front and move parallel to isobaths between depths of 2 to 6 m. This is essentially the reverse flow from the prefrontal regime (compare with Figure 4B).

Strong northeasterly post-frontal winds begin on December 26 (Figure 3A) and force the plume water offshore by December 27 (Figure 6B). The wind has rotated to northwesterly by December 27 (2308 hours) and continues to push the river plume offshore. The river plume mixes with offshore water as it is transported eastward (Figure 6C), resulting in salinities of 10–20 psu over a large part of the shelf. The strongest surface currents (0.5–0.8 m s^{-1}) at this time (Figures 7B and 7C) are generated over the shoals at 91.8°W, 92.2°W, and in the southeast corner of the domain. These locations coincide with the strongest salinity fronts (Figures 6B and 6C). It appears that, despite the offshore wind, bathymetry is constraining the movement of the plume due to the large density differences between it and the offshore water. The baroclinic gradients appear to block the less dense plume water from moving into deeper water at certain locations, thus creating weaker currents (0.1–0.3 m s^{-1}) between the very intense and localized offshore directed flows (Figures 7B and 7C).

The cold front of December 29 reinforces the overall effect of the first front in the NCOM simulation. High-salinity shelf water is pushed closer to the coast, and the river plume is transported farther to the east or back into Atchafalaya Bay. By December 30, the northwesterly post-frontal winds of the

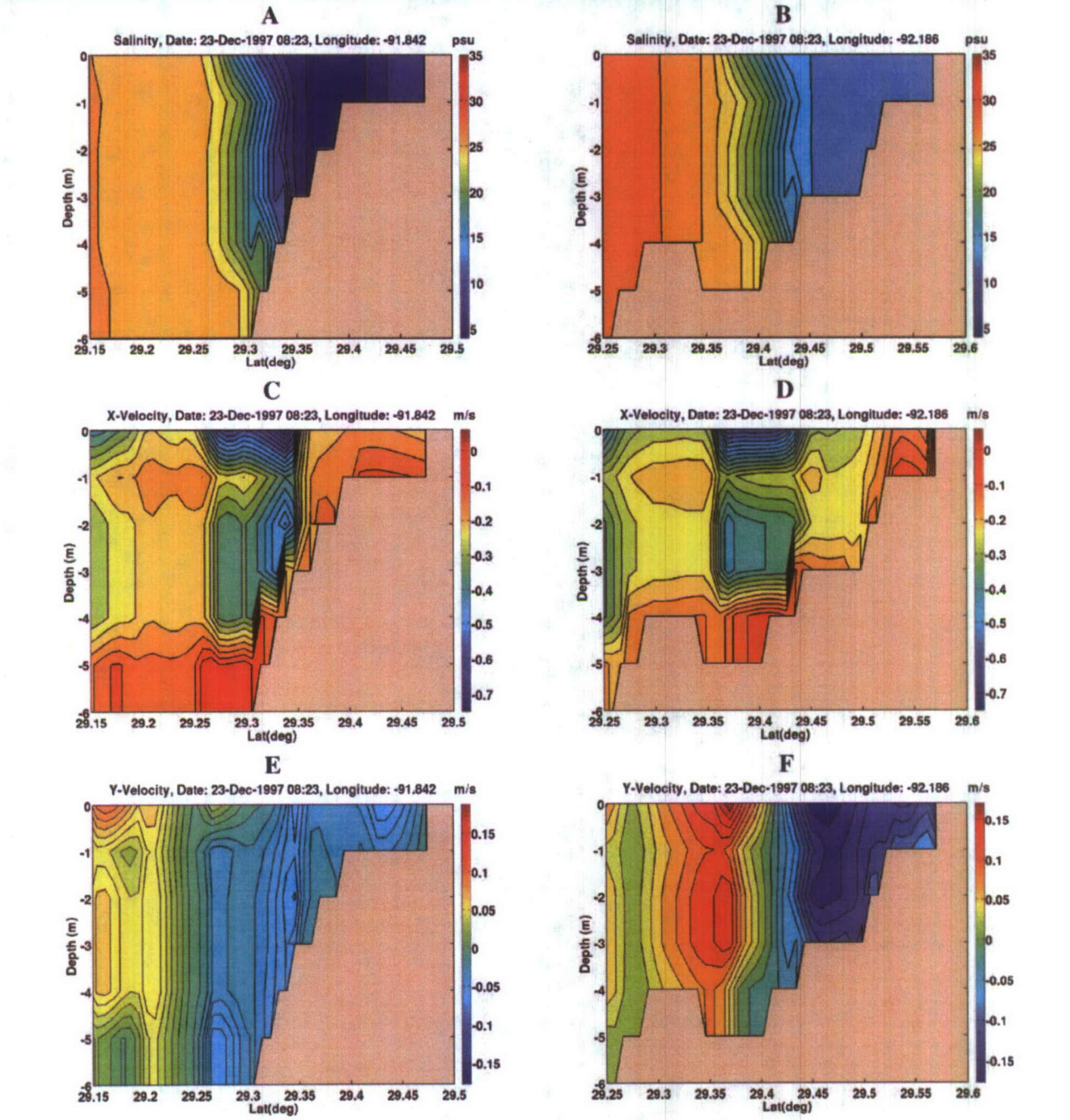

Figure 5. T1 and T2 cross-shore transects of salinity (A and B), alongshore velocity (C and D), and cross-shore velocity (E and F) on December 23 (0823 hours), 1997. See Figure 2B for the locations of T1 and T2. The displayed cross-shore width and offshore depth is the same for both transects (which span different latitudes). The offshore depths are not shown in order to focus on the narrow salinity front created by the river plume. The model results are interpolated to 1-m depth increments. Positive x and y velocities are to the east and the north, respectively.

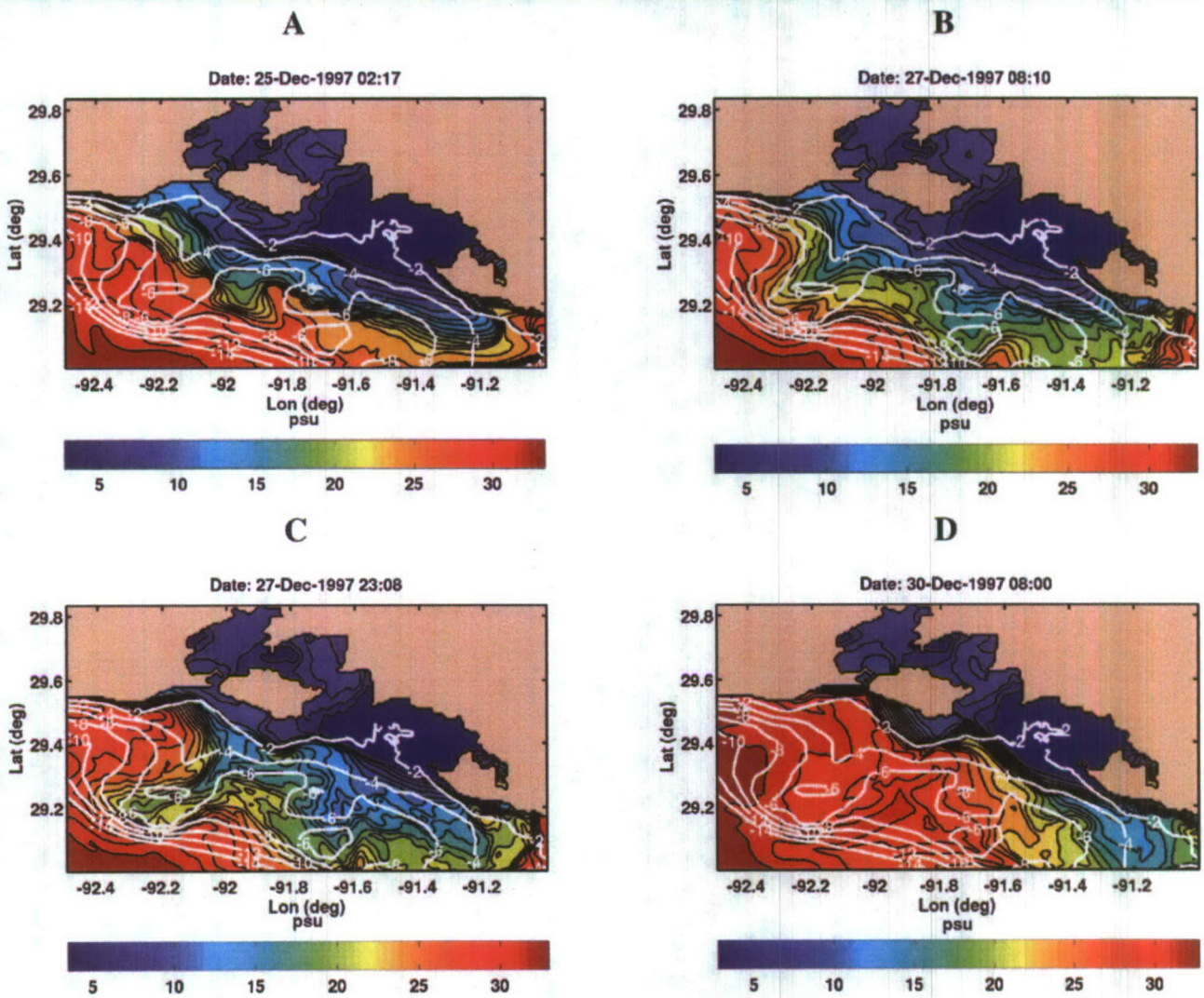

Figure 6. Surface salinity and bathymetry contours. (A) December 25 (0217 hours) during the passage of the front (westerly winds) (B) December 27 (0810 hours) during the post-frontal northeasterly winds. (C) December 27 (2308 hours) during the post-frontal northwesterly winds. (D) December 30 (0800 hours) during the second time period of post-frontal northwesterly winds (second cold front). Note that the bathymetry contours from −2 to −14 m are in white with 2-m intervals.

second front continue to push the river plume toward the southeast corner of the domain (Figure 6D). The surface flow at this time is primarily to the southeast with the strongest currents directly associated with the river plume (Figure 7D).

The surface salinity distribution of the plume during the first cold front is consistent with SSC estimated from AVHRR data (WH00). For example, the remotely sensed sediment plume on December 29 extended offshore beyond the 10-m isobath and quite far to the southeast as well. The correlation between the high values of SSC and the southeast location of the plume predicted by NCOM (see CKW1 for a discussion and a revised version of the image from WH00) in Figure 6D indicates that the currents and salinities from the simulation are reasonably similar to the actual circulation.

Offshore salinity measurements are not available for the time period of this study, but observations during other fronts reveal post-frontal salinity contours that are qualitatively similar to those shown in Figures 6C and 6D (KINEKE *et al.*, 2006). These observations suggest that 32-psu shelf water approaches Southwest Pass from the west and that lower salinity water (10–25 psu) moves offshore along the shoals just as the model predicts. These post-frontal field observations of salinity supplement the model results that the bathymetry strongly influences the shelf circulation during cold fronts.

Current measurements are not available for the shelf during the study interval, but offshore currents were measured at several locations in water depths up to 50 m during an earlier cold front as discussed in WH00. Post-frontal south-

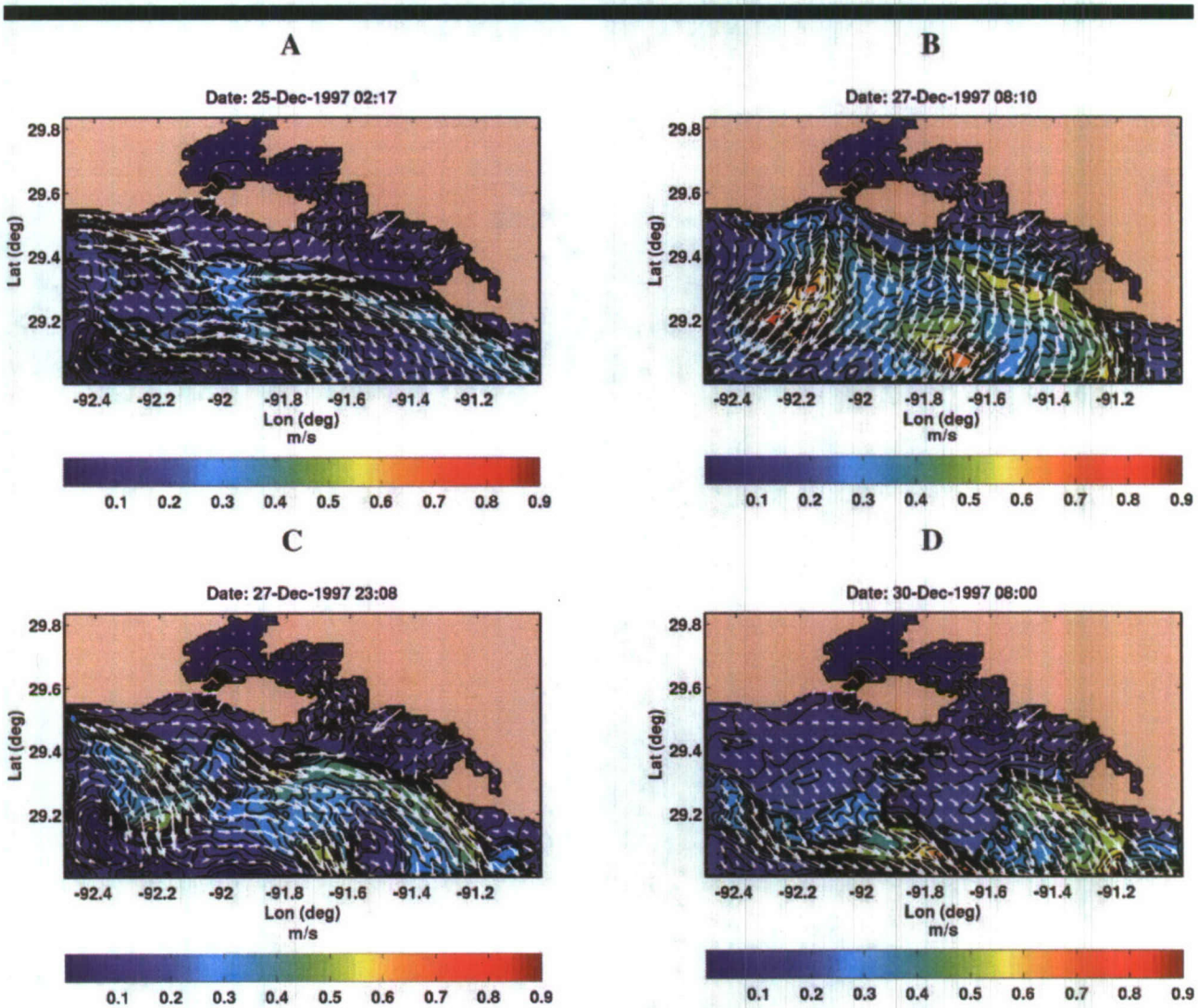

Figure 7. Surface current velocity: magnitude and direction. (A) December 25 (0217 hours) during the passage of the front (westerly winds). (B) December 27 (0810 hours) during the post-frontal northeasterly winds. (C) December 27 (2308 hours) during the post-frontal northwesterly winds. (D) December 30 (0800 hours) during the second time period of post-frontal northwesterly winds (second cold front). Every sixth current vector is plotted. Note: Same calendar dates as Figure 6 are plotted.

eastward currents of 0.3 to 0.6 m s^{-1} were observed close to the 10-m isobath south of Marsh Island at a depth of 3 m. These currents were similar in direction and magnitude to the offshore surface currents predicted by the model (Figures 7C and 7D) as well as the post-frontal currents of the third cold front (not shown). WALKER *et al.* (2002) reported maximum southeastward currents south of Marsh Island of 0.5–0.7 m s^{-1} for several hours and a daily averaged middepth current of 0.3 m s^{-1} during a cold-front passage event in March 2001. Observed post-frontal sediment transport patterns (HUH, WALKER, and MOELLER, 2001; MOELLER *et al.*, 1993; WH00; WALKER *et al.*, 2002) are also consistent with the model results. These comparisons provide us with a benchmark for the post-frontal currents on the shelf and indicate that the model is predicting realistic post-frontal offshore currents.

Across-Shore Structure

During the cold front of December 25, the predicted surface plume is displaced offshore as a thin layer of low-salinity water (Figure 8). Along transect T1 (Figures 8A and 8C), high-salinity water is predicted between this surface layer and a low-salinity tongue at a depth of 3 m. The deeper low-salinity water separates from the plume as it moves offshore and forms subsurface prisms of low-salinity water along the plume front. Shelf water is also moving shoreward near the bottom as the lower salinity water moves seaward. The in-

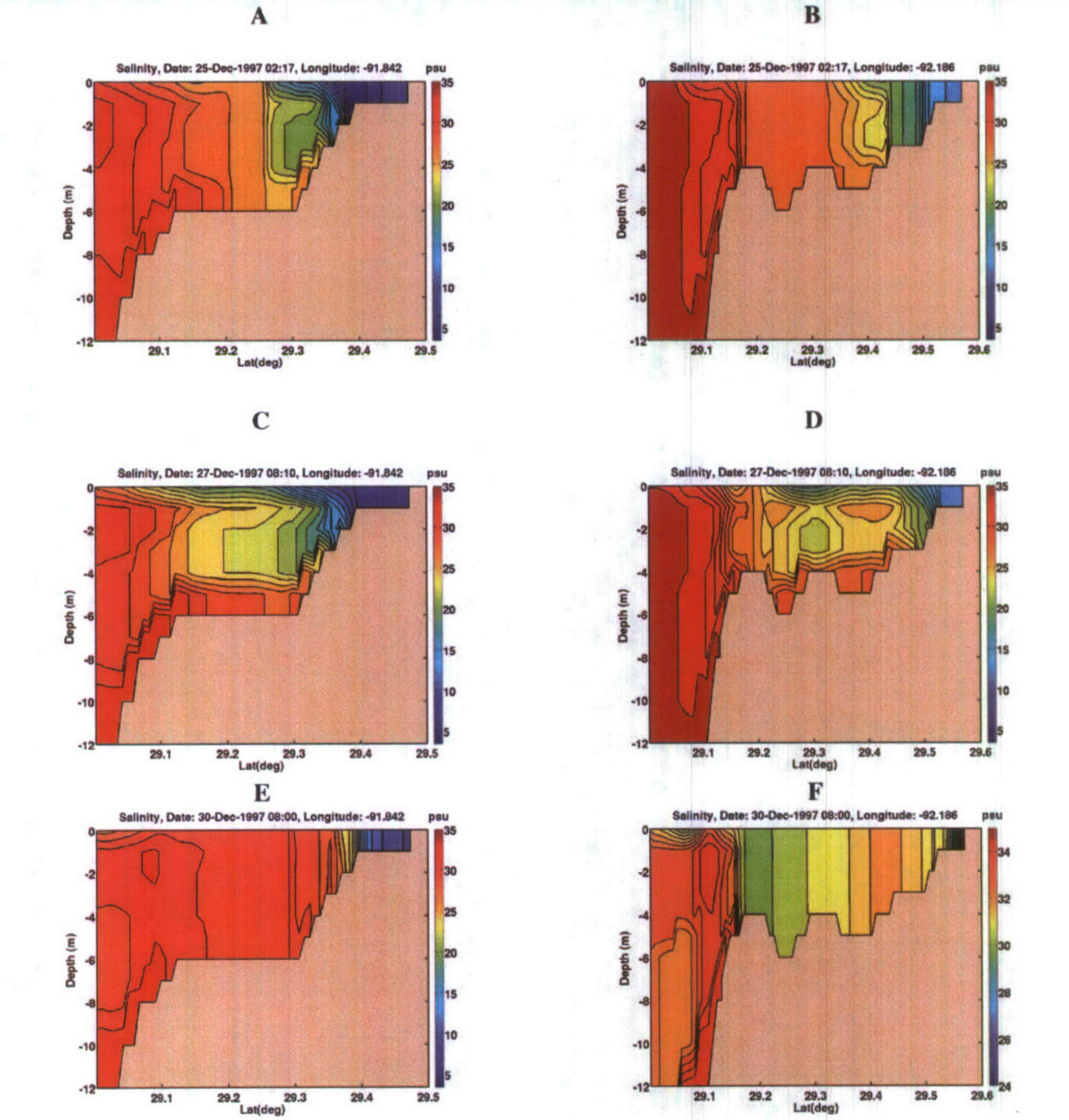

Figure 8. Predicted salinity at transects T1 (left column) and T2 (right column) for the cold front of December 25. Panels A and B are predicted for December 25, panels C and D are predicted on December 27, and panels E and F are predicted for December 30. The times used for these transects are the same as those used for the surface salinity in Figure 6. The salinity range is the same for all of the figures except (F). These transects are plotted over the same depth range from 0 to −12 m. See Figure 2B for the transect locations.

trusion of high-salinity water near the northwestern corner of the model domain (Figure 6B) is also seen in transect T2 (Figures 8B and 8D), which also shows a tongue of freshwater moving seaward along the bathymetric shoal. Higher salinity water (higher than the salinity at the surface) is actually moving around this tongue of freshwater below the surface water. Shelf water approaches the coast by December 30 (Figure 6D) and produces a well-mixed water column at both transect T1 (Figure 8E) and transect T2 (Figure 8F) in water depths less than 6 m. The residual plume water remains at the surface while the plume itself has been pushed against the coast to depths of about 1 m. In depths greater than 6 m, the water column retains some of the stratification that was generated during the passage of each front.

These model results cannot be compared directly with data, but the salinity transects at T1 and T2 are in qualitative agreement with hydrographic measurements by ALLISON *et al.* (2000). Their observations show the displacement of the plume water offshore by strong cold-front winds and the increase in stratification on the shelf (Figure 8C). Their observations also show a well-mixed salty water column after a cold front as predicted by the model (Figures 8E and 8F). This supports the post-frontal circulation pattern predicted by the model (Figure 6D) in which high-salinity shelf water moves close to the shore. These model results are also supported by the surface salinity measurements discussed above (KINEKE *et al.*, 2006).

Alongshore Structure

The post-frontal winds generate a predicted westward surface jet with speeds from 0.2 to 0.4 m s^{-1}, which transports the plume offshore to the southwest (Figure 6B). The currents weaken below 1 m but remain to the southwest (Figure 9). The predicted near-bottom flow is eastward and shoreward, however, with magnitudes of less than 0.05 m s^{-1}. This upwelling-favorable circulation pattern during the post-frontal period has been observed by KINEKE *et al.* (2006), who reported offshore currents of 0.3 m s^{-1} in the upper part of the water column and onshore currents of 0.1 m s^{-1} at 1 m above the bottom.

The plume is extensive at the surface (Figure 10A), but it remains confined to shallower water as it moves seaward; the results presented in Figure 10 are along transect T3 (see Figure 2B). Low-salinity water is predicted over the shore-oblique shoals on the inner shelf (Figure 2B), where weak subsurface jets flow seaward (Figure 10B) at 3 m below the surface. These tubes of freshwater are part of the same phenomenon discussed above (Figures 8C and 8D). The regions of freshwater at 3-m depth seen in Figure 10A can become detached from the plume as higher salinity water entrains them. Another important point to make about the alongshore structure on the inner shelf pertains to the influence of bathymetric gradients. The offshore jets develop over the bathymetric shoals at 92.2°W and 91.6°W, whereas much weaker offshore flow is predicted between them. The bathymetric gradients generate baroclinic forces as discussed above, which prevent the freshwater from moving offshore at these locations; thus the currents are small and the salinity

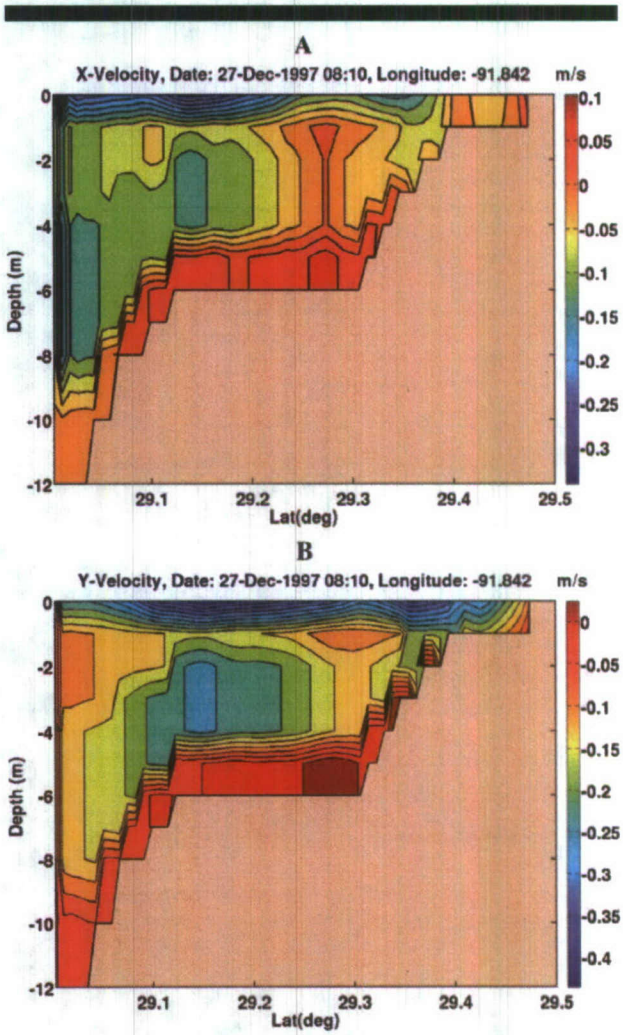

Figure 9. Current velocities at cross-shore transect T1 during post-frontal northeasterly winds (December 27): (A) Alongshore component; (B) Cross-shore component. Negative x and y velocities are to the west and south respectively. See Figure 7B for the surface currents over the entire domain at this time. See Figure 2B for transect location.

is much higher. Furthermore, the alongshore velocities (Figure 10C) are generally larger at the surface between the offshore jets (*e.g.*, at 91.8°W). This pattern corresponds to the strong currents moving parallel to the bathymetry at these locations (Figure 7C).

SALINITY FRONTS IN THE WESTERN BAYS

The predicted salinity from the model has been compared with observations in West Cote Blanche Bay and Vermilion Bay in a previous paper (CKW1), and the model results were overall quite good but with some systematic errors. The salinity at both of these locations is determined by the bathymetry, wind forcing, astronomical tides, and river input, which together make it problematical to elucidate the individual effects of these factors. This section will, therefore, discuss the

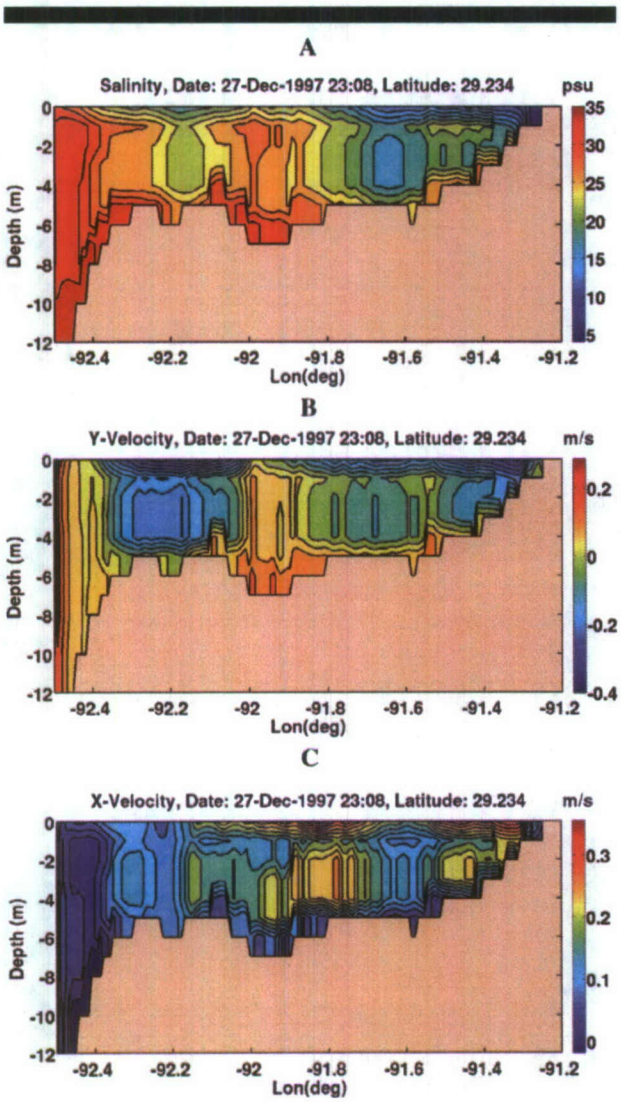

Figure 10. Salinity and currents along transect T3 during post-frontal northwesterly winds (December 27): (A) salinity, (B) cross-shore velocity, and (C) alongshore velocity. See Figure 2B for the transect location. The alongshore and cross-shore velocities are negative if they are directed to the west and the south, respectively. The transect is oriented looking onshore.

hydrographic processes that determine the salinity variations observed and predicted at these locations.

West Cote Blanche Bay

The low salinity in West Cote Blanche Bay during southerly winds (Figure 11A) results from movement of the Atchafalaya plume to the northwest. Prior to the first cold front, the simulated river plume (Figure 11A) intrudes into West Cote Blanche Bay and lowers the salinity at site 1 to less than 6 psu (arrow 1 in Figure 12). The water level at site 1 increases during these prefrontal winds (arrow 1 in Figure 12). Conversely, the post-frontal northerly wind pushes the river plume in a southeastward direction and water from the western bays is transported eastward (Figure 11B), resulting in lowered water levels throughout the bay system (CKW1). After both of these cold fronts have passed (Figure 11B), the higher salinity water of West Cote Blanche Bay (approximately 8 psu) has been displaced to the entrance of East Cote Blanche Bay and the salinity at site 1 has increased to 7.8 psu. In addition, the low-salinity water of Vermilion Bay is intruding into West Cote Blanche Bay from the northwest. The water level reaches a minimum and the salinity reaches its maximum at site 1 during the post-frontal winds (arrow 2 in Figure 12); the salinity and water level at site 1 are therefore anticorrelated during all three cold-front events.

The predicted salinity at site 1 reaches a minimum of 4 psu on January 3, which is about 36 hours after the maximum water level. The predicted water level subsequently decreases rapidly as the salinity increases. The rapid changes in the salinity and water level during this interval correspond to the strengthening of the plume's westward transport. It takes several days to reestablish the plume's westward extent under the steady southeasterly wind forcing because it was displaced far to the southeast by the first two cold fronts (Figure 6D). When the westward transport is finally reestablished, the water levels of the western bays decrease sharply on January 5. This process advects the salinity front toward East Cote Blanche Bay and thereby increases the salinity at site 1.

In order to achieve reasonably good agreement between the model results and the data of WH00 at site 1 it was necessary to control the salinity of West Cote Blanche Bay through the Jaws Bay GIWW outlet. Although this might appear to be a rather unrealistic approach, it was necessary due to the relatively short spin-up time of the model from July 1997 to November 1997. The exact processes that lead to the high salinity values in the data (~8 psu) are still uncertain, but it is clear from the hydrodynamics that the higher salinity water at site 1 must originate from the western bays during a cold-front event.

It should also be pointed out that the net exchange of water between West Cote Blanche Bay and other areas of the bay system, as well as the shelf, appears to be rather weak based on the model results of Figure 11. The water in this bay (and hence the salinity front) is displaced westward and eastward by the wind and the tides, but the overall transport of water does not appear great. This would suggest that higher salinity water intrudes from Vermilion Bay (as seen in the next section) or on the eastern side of Marsh Island when the river plume is displaced to the east. In addition, since the exchange is weak and the sources of freshwater within the western bays are relatively small in their volumetric transport, the water in West Cote Blanche Bay could become more saline over time through evaporation (a process not accounted for in this simulation).

Vermilion Bay

Site 3 experiences large salinity fluctuations during cold fronts because it is located near the entrance to Southwest Pass in Vermilion Bay. The measured salinity at site 3 ranged from 1.6 to 16.8 psu during the study interval

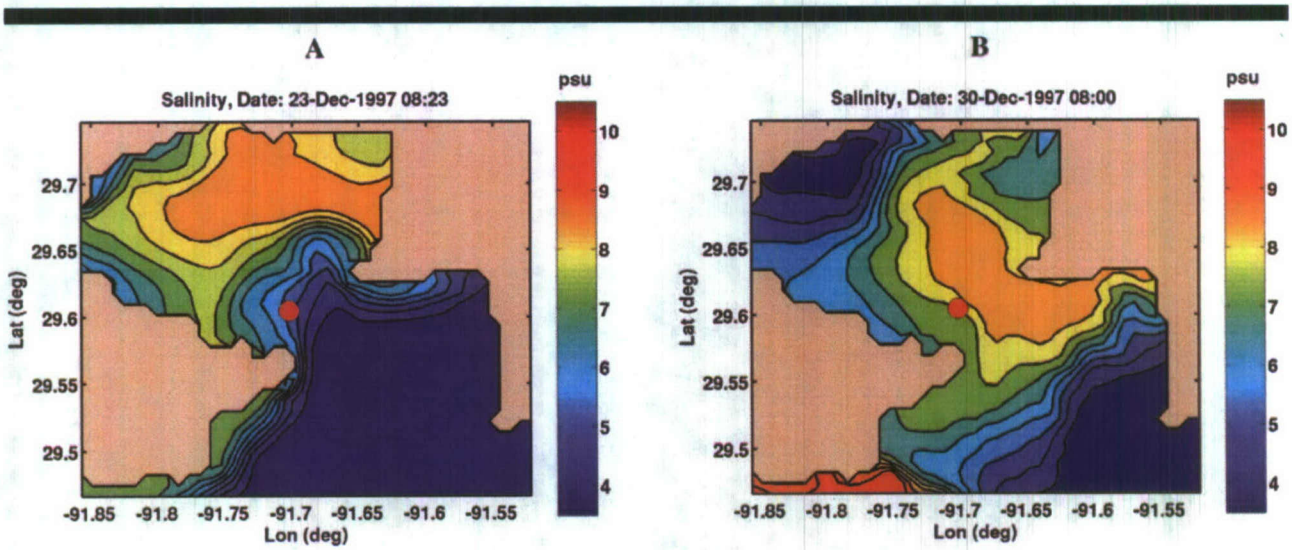

Figure 11. Predicted salinity contours on (A) December 23 (0823 hours) prior to the passage of the first cold front (northeasterly winds) (see Figure 4A for entire domain). (B) December 30 (0800 hours) at the end of the second cold front (northwesterly winds) (see Figure 6D for entire domain). The red circle indicates the location of site 1. The salinity range is 3.5 to 10.5 psu.

(WH00). This variability is caused by the inflow of high-salinity water through Southwest Pass (WH00), but the details of this process have not been fully captured by previous measurements. The flood tide currents on January 1 (Figure 13A) are opposed by a northeasterly wind of 5 m s^{-1}, which rotates to southeasterly as the tide changes to ebb. High-salinity shelf water enters Southwest Pass on December 30 (Figure 6D) and produces a sharp salinity front at its entrance (Figure 13A). Low-salinity water is subsequently advected to site 3 during the ebb tide (Figure 13B).

The maximum incoming or outgoing currents at site 3 (Figure 14) precede an increase (arrow 1) or decrease (arrow 2) in salinity. Note that the current velocity at site 3 is projected along a 30°/210° axis and the current is positive if it is flowing into Vermilion Bay. Large salinity fluctuations occur after each cold front when high-salinity water enters Southwest Pass and the currents are primarily tidal in nature. This shows quite clearly that high-salinity water is being transported into the vicinity of site 3 during the flood tide and that stronger incoming currents produce larger salinity values at site 3. The minimum salinity values during these post-frontal periods do not vary nearly as much since they are being determined by the water within Vermilion Bay. The predicted incoming currents at site 3 increase during the cold fronts (Figure 14) and increase the transport of shelf water into Vermilion Bay. Outflowing currents dominate at site 3 during the first week of January and the salinity is lower. Tidal incoming currents, which are coincidentally larger during the cold fronts, are enhanced by the offshore circulation at the end of each cold-front cycle. However, the outgoing tidal currents dominate between the cold fronts because the southeasterly winds raise the water levels of the western bays.

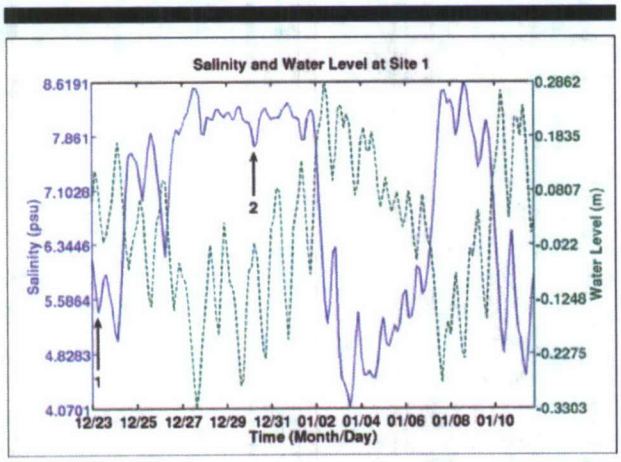

Figure 12. Salinity (solid line) and water level (dashed line) with the mean removed at site 1 in West Cote Blanche Bay between December 23, 1997, and January 11, 1998. The time indicated by arrow 1 corresponds to Figure 11A, and arrow 2 indicates the time in Figure 11B.

The duration and strength of a cold front determine the magnitude of the salinity fluctuations at site 3. The weak cold front of January 7 generates smaller fluctuations in the predicted salinity relative to the first two cold fronts (Figure 15). The January 7 cold front does not push high-salinity shelf water into Southwest Pass as during the previous front (December 29) and, therefore, the peak salinity at SW1 is significantly smaller. The tide-dominated currents at site 3 (Figure 14) have approximately the same magnitude during the second and third cold fronts, and consequently it is the offshore circulation that determines the salinity at site 3.

SUMMARY AND CONCLUSION

As discussed in CKW1, a strong correlation was found to exist between the remotely sensed SSC (HUH, WALKER, and

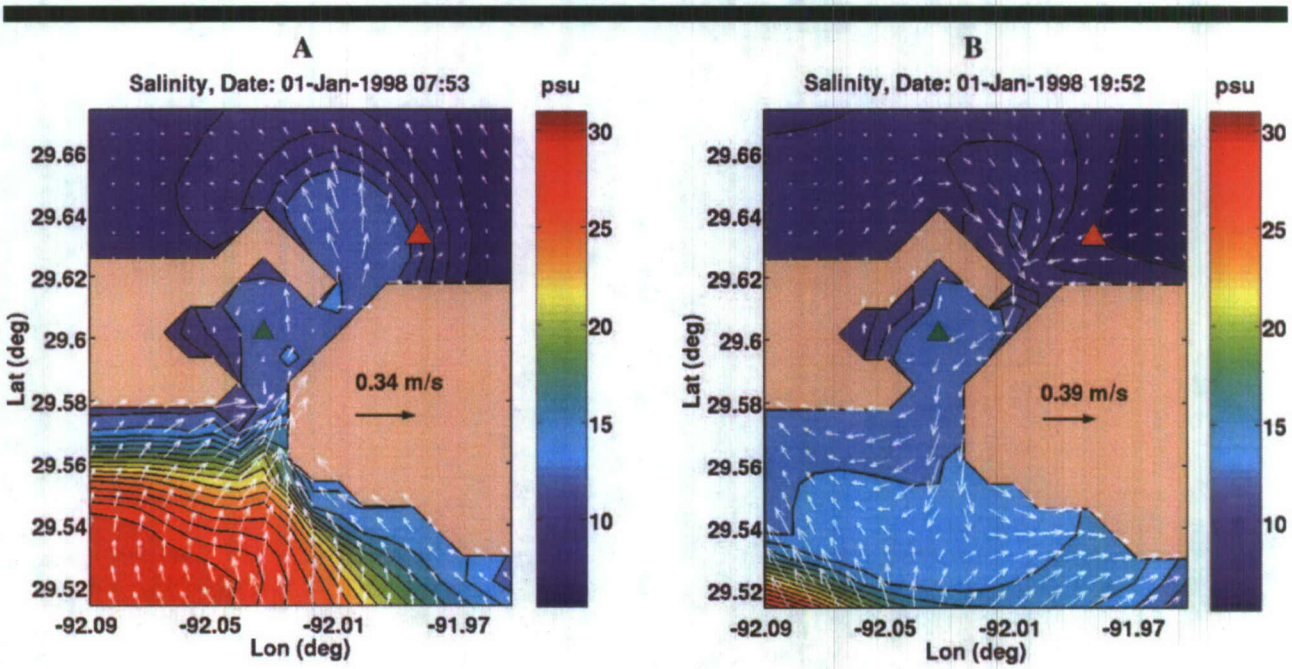

Figure 13. Predicted salinity contours during January for Southwest Pass. (A) Incoming flood tide currents from NCOM. (B) Outgoing ebb tide currents from NCOM. The red and green triangles indicate the locations of site 3 (see Figure 2B for its location) and SW1, respectively. Salinity ranges from 5.5 to 31 psu.

MOELLER, 2001; MOELLER *et al.*, 1993; WH00) and the surface salinity patterns predicted by NCOM since the fine grain sediment acts as a tracer for the lower salinity water of the plume. This behavior is also consistent with field measurements by KINEKE *et al.* (2006) of salinity and SSC in this region following a cold-front event and during the westward transport of plume water. Being able to predict how the freshwater plume and overall offshore salinity patterns are affected by cold-front winds is therefore essential to understanding the sediment deposition, resuspension, and transport processes of the region. In addition, the ability to accurately model the westward flow of the river plume is a crucial first step toward predicting the large quantities of sediment that

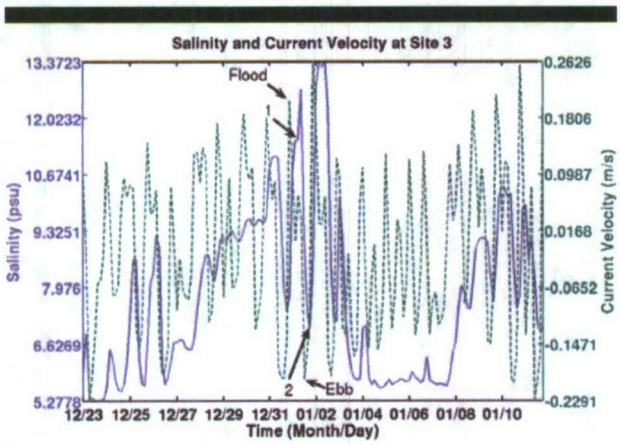

Figure 14. Salinity (solid line) and current velocity (dashed line) time series at site 3. The current velocity of the model is projected along 30°/210°, and the current is positive if it is flowing into Vermilion Bay. The flood and ebb current velocities are indicated with arrows. Arrows 1 and 2 indicate the salinity values during the flood and ebb tides shown in Figure 13, respectively.

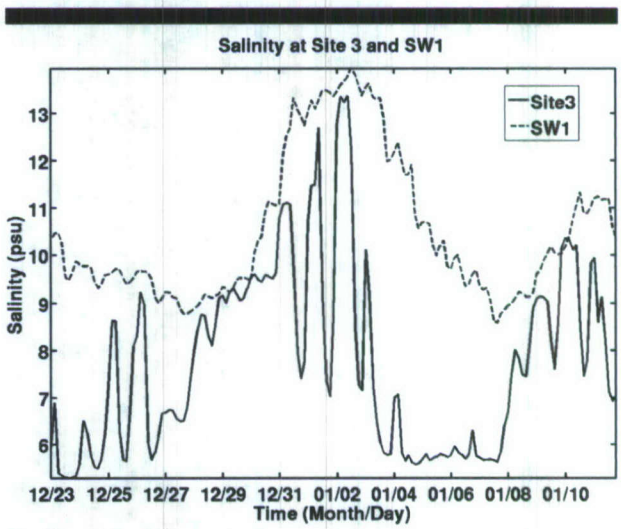

Figure 15. Salinity time series at site 3 and SW1. See Figure 13 for location of SW1.

are transported to the Chenier Plain of western Louisiana (WELLS and KEMP, 1981).

The westward transport of the model's river plume has the general characteristics of a surface-to-bottom type plume with horizontal stratification and strong alongshore currents at the plume front. Because the plume becomes "trapped" at a particular cross-shore depth it moves westward parallel to the alongshore bathymetric contours (CHAPMAN and LENTZ, 1994). This also leads to a convergence zone at the plume front where the cross-shore currents go to zero and then change direction. These particular features of the Atchafalaya river plume have not been addressed in the literature to our knowledge and need to be investigated further through modeling and field studies.

The analysis of the horizontal and vertical circulation during a cold-front event reveals a number of complex circulation processes occurring along the shelf that had not been discussed previously. In particular, the offshore transport and mixing of the plume water over bathymetric shoals have not been realized until this study. The evolution of the vertical salinity during a cold front revealed that prisms of freshwater are generated at the plume front as well. These prisms of freshwater can become detached from the main plume and transported farther offshore. The vertical structure of the currents reveals a highly sheared offshore surface layer and onshore directed bottom currents. Based on recent observations, these bottom currents appear to be a significant source of onshore sediment transport (KINEKE *et al.*, 2006). More field measurements are required to adequately validate the predicted vertical structure of the circulation on the shelf during cold-front events.

Because the shelf bathymetry plays an important role in determining the plume motion, it will also affect the sediment transport. It is clear from the results of this study that the observed sediment transport to the west and southeast (HUH, WALKER, and MOELLER, 2001; WH00; WALKER *et al.*, 2002), which occurs under easterly and westerly winds, respectively, are two examples of the river plume moving parallel to the alongshore bathymetry. The narrowing of the river plume as it moves west also accounts for the high SSC observed along the coast of the Chenier Plain (KINEKE *et al.*, 2006). In addition, our results indicate that the bathymetric shoals can act as conduits for sediment transport because low-salinity water moves offshore over them. Remotely sensed images and field observations of SSC are consistent with this hypothesis as well (KINEKE *et al.*, 2006; WH00); however, because the plume motion occurs rapidly and over a large area during cold fronts, it is difficult to recognize this behavior using only field observations or remotely sensed images.

This study has focused on the large-scale circulation of the Atchafalaya and Wax Lake Outlet river plumes during the passage of multiple cold fronts. The goal of this work was to investigate the three-dimensional baroclinic circulation of the river plume during its two distinct circulation modes in the winter months: (1) westward transport and (2) cold-front–induced motion. A more fundamental understanding of the horizontal and vertical salinity and current structure is essential for determining the sediment transport to the Chenier Plain as well as the cold-front–induced transport of river plume and resuspended sediment. Because the large quantities of sediment transported by the river plume impact the entire region it is imperative that coastal managers have a better understanding of the river plume dynamics.

The hydrodynamic circulation of this region had not been simulated with a fully baroclinic model prior to this study, and there are many aspects of the shelf circulation that had not been fully appreciated. The most important aspects of the shelf circulation revealed by our study are the influence of bathymetry on the plume's motion and the complexity of the horizontal circulation throughout the water column. It is apparent from these results that sediment transport within the region is complex because it depends on the vertical structure of both the currents and salinity.

This work also encourages a greater integration of numerical modeling and field studies. Field data are required to validate models, and models can be used to understand large-scale processes in ways that are not possible through regional field studies alone. As seen from our analysis of the salinity at sites 1 and 3, it is necessary to have multiple data sites and multiple types of data to determine the dominant circulation processes at a particular location. In order to apply numerical models such as NCOM for the purpose of coastal management, more complete spatial and temporal data sets will be required in the future.

ACKNOWLEGMENTS

Cobb and Keen were funded by program element 0601153N of the Office of Naval Research. The authors would like to acknowledge Lucy Smedstad for providing the global NCOM boundary conditions required for this study and Paul Martin for help with constructing the Atchafalaya computational grid. In addition we would also like to acknowledge Clark Rowley and Charlie Barron for assistance with the riverine input of NCOM. The U.S. Army Corps of Engineers New Orleans Division funded the field measurements that were used extensively for model validation.

LITERATURE CITED

ALLISON, M.A.; KINEKE, G.C.; GORDON, E.S., and GONI, M.A., 2000. Development and reworking of a seasonal flood deposit on the inner continental shelf off the Atchafalaya River. *Continental Shelf Research*, 20, 2267–2294.

BARRON, C.N.; SMEDSTAD, L.F.; RHODES, R.C.; KARA, A.B.; ROWLEY, C.R.; ALLARD, R.A., and HURLBURT, H.E., 2004. Validation of the 1/8° global Navy coastal ocean model nowcast/forecast system. *NAVO MSRC Navigator*, Spring 2004, 5–8.

CHAPMAN, D.C. and LENTZ, S.J., 1994. Trapping of a coastal density front by the bottom boundary layer. *Journal of Physical Oceanography*, 24, 1464–1479.

COBB, M.; KEEN, T.R., and WALKER N.D., 2008. Modeling the circulation of the Atchafalaya Bay region, 1: model description and validation. *Journal of Coastal Research*, 24, 1036–1047.

DRAUT, A.E.; KINEKE, G.C.; HUH, O.K.; GRYMES, J.M., III; WESTPHAL, K.A., and MOELLER, C.C., 2005a. Coastal mudflat accretion under energetic conditions, Louisiana Chenier-Plain coast, USA. *Marine Geology*, 214, 27–47.

DRAUT, A.E.; KINEKE, G.C; VELASCO, D.W.; ALLISON, M.A., and PRIME, R.J., 2005b. Influence of the Atchafalaya River on the recent evolution of the Chenier-Plain inner continental shelf, northern Gulf of Mexico. *Continental Shelf Research*, 25, 91–112.

HUH, O.K.; ROBERTS, H.H.; ROUSE, L.J., JR., and RICKMAN, D.A.,

1991. Fine grain sediment transport and deposition in the Atchafalaya and Chenier Plain sedimentary system. *In: American Society of Civil Engineers Proceedings from Coastal Sediments '91* (Seattle, Washington), pp. 817–830.

HUH, O.K.; WALKER, N.D., and MOELLER, C., 2001. Sedimentation along the Eastern Chenier Plain coast: down drift impact of a delta complex shift. *Journal of Coastal Research,* 17, 72–81.

KAHN, J.H. and ROBERTS, H.H., 1982. Variations in storm response along a microtidal transgressive barrier-island arc. *Sedimentary Geology,* 33, 129–146.

KARA, A.B.; BARRON, C.N.; MARTIN, P.J.; SMEDSTAD, L.F., and RHODES, R.C., 2006. Validation of interannual simulations from the 1/8° global Navy Coastal Ocean Model (NCOM). *Ocean Modeling,* 11, 376–398.

KEEN, T.R.; KO, D.S.; SLINGERLAND, R.L.; RIEDLINGER, S., and FLYNN, P., 2006. Potential transport pathways of terrigenous material in the Gulf of Papua. *Geophysics Research Letters,* 33, L04608, doi: 10.1029/2005GL025416.

KEMP, G.P.; WELLS, J.T., and VAN HEERDEN, I.L., 1980. Frontal passages affect delta development in Louisiana. *Coastal Oceanography and Climatology News,* 3, 4–5.

KINEKE, G.C.; HIGGINS, E.E.; HART, K., and VELASCO, D., 2006. Fine-sediment transport associated with cold-front passages on the shallow, Gulf of Mexico. *Continental Shelf Research,* 26, 2073–2091.

KO, D.S.; PRELLER, R.H., and MARTIN, P.J., 2003. An experimental teal-time intra-Americas sea ocean nowcast/forecast system for coastal prediction. *In: Fifth Conference on Coastal Atmospheric and Oceanic Prediction and Processes,* American Meteorological Society, Boston, Massachusetts.

KOURAFALOU, V.H.; OEY, L.-Y.; WANG, J.D., and LEE, T.N., 1996. The fate of river discharge on the continental shelf 1. Modeling the river plume and the inner shelf coastal current. *Journal of Geophysical Research,* 101(C2), 3415–3434.

MOELLER, C.C.; HUH, O.K.; ROBERTS, H.H.; GUMLEY, L.E., and MENZEL, P.W., 1993. Response of Louisiana coastal environments to cold front passage. *Journal of Coastal Research,* 9, 434–447.

MOREY, S.L.; MARTIN, P.J.; O'BRIEN, J.J.; WALLCRAFT, A.A., and ZAVALA-HIDALGO, J., 2003. Export pathways for river discharged fresh water in the northern Gulf of Mexico. *Journal of Geophysical Research,* 108: doi: 10.1029/2002JC001674.

MOSSA, J. and ROBERTS, H.H., 1990. Synergism of riverine and winter storm-related sediment transport processes in Louisiana's coastal wetlands. *Gulf Coast Association of Geological Societies,* 40, 635–642.

NARAYANAN, C. and GARVINE, R.W., 2002. Large scale buoyancy driven circulation on the continental shelf. *Dynamics of Atmospheres and Oceans,* 36, 125–152.

OEY, L.-Y. and MELLOR, G.L., 1993. Subtidal variability of estuarine outflow, plume, and coastal current: a model study. *Journal of Physical Oceanography,* 23, 164–171.

PEREZ, B.C.; DAY, J.W., JR.; ROUSE, L.J.; SHAW, R.F., and WANG, M., 2000. Influence of Atchafalaya River discharge and winter frontal passage on suspended sediment concentration and flux in Fourleague Bay, Louisiana. *Estuarine, Coastal, and Shelf Science,* 50, 271–290.

ROBERTS, H.H.; ADAMS, R.D., and CUNNINGHAM, R.H.W., 1980. Evolution of sand dominant subaerial phase, Atchafalaya Delta, Louisiana. *American Association of Petroleum Geologists Bulletin,* 64, 264–279.

ROBERTS, H.H.; HUH, O.K.; HSU, S.A.; ROUSE, L.J., and RICKMAN, D.A., 1987. Impact of cold-front passages on geomorphic evolution and sediment dynamics of the complex Louisiana coast. *In: American Society of Civil Engineers Proceedings of Coastal Sediments '87,* pp. 1950–1963.

ROBERTS, H.H.; HUH, O.K.; HSU, S.A.; ROUSE, L.J., JR., and RICKMAN, D.A., 1989. Winter storm impacts on the Chenier Plain coast of Southwestern Louisiana. *Transactions of the Gulf Coast Association of Geological Societies,* 39, 515–522.

SCHLEMON, R.J., 1975. Subaqueous delta formation—Atchafalaya Bay, Louisiana. *In*: BROUSSARD, M.L. (ed.), *Deltas: Models for Exploration.* Houston, Texas: Houston Geological Society, pp. 209–221.

VAN HEERDEN, I.L. and ROBERTS, H.H., 1980. The Atchafalaya Delta—Louisiana's new prograding coast. *Transactions of the Gulf Coast Association of Geological Societies,* 30, 497–506.

WALKER, N.D., 2001. Tropical and extra-tropical storm impacts on circulation, sediment, and salt flux: Atchafalaya-Vermilion Bay region, Louisiana coast. *Estuaries,* 24, 498–508.

WALKER, N.D. and HAMMACK, A.B., 2000. Impacts of winter storms on circulation and sediment transport: Atchafalaya-Vermilion Bay region. *Journal of Coastal Research,* 16, 996–1010.

WALKER, N.D.; ROBERTS, H.; STONE, G.; BENTLEY, S.; HUH, O.; SHEREMET, A.; ROUSE, L.; INOUE, M.; WELSH, S.; HSU, S.A., and MYINT, S., 2002. Satellite-based assessment of sediment transport, distribution and resuspension associated with the Atchafalaya River discharge plume. *Gulf Coast Association of Geological Societies Transactions,* 52, 967–973.

WELLS, J.T. and KEMP, P.W., 1981. Atchafalaya mud stream and recent mudflat progradation: Louisiana Chenier Plain. *In: Gulf Coast Association of Geological Societies Transactions,* 31st Annual Meeting (21–23 October, Corpus Christi, Texas), pp. 409–416.

XING, J. and DAVIES, A.M., 1999. The effect of wind direction and mixing upon the spreading of a buoyant plume in a non-tidal regime. *Continental Shelf Research,* 19, 1437–1483.